Supplementary Materials for:

Tumor aneuploidy correlates with markers of immune evasion and with reduced response to immunotherapy

Teresa Davoli[1], Hajime Uno [2] , Eric C. Wooten[1] & Stephen J. Elledge[1*]

[1]Howard Hughes Medical Institute, Department of Genetics, Harvard Medical School, Division of Genetics, Brigham and Women's Hospital, Boston, MA 02115, USA

[2] Dana-Farber Cancer Institute, Boston, MA 02215-5450, USA

*Corresponding author. Email: selledge@genetics.med.harvard.edu

This PDF file includes:

Figs. S1 to S9

Legends to Tables S1 to S6

Fig. S1

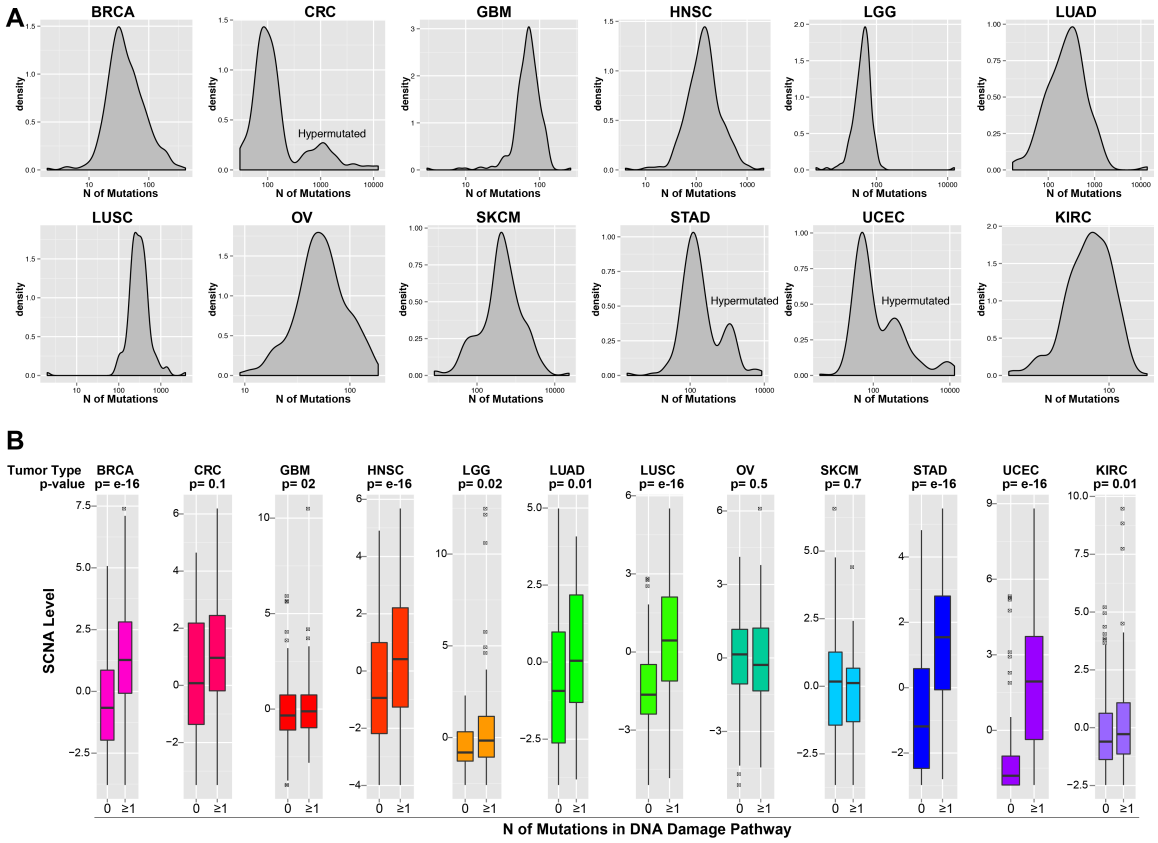

Figure S1

Distribution of mutations across tumor types and relationship between SCNA level and number of driver mutations in DNA damage pathway

(A) Distribution of the number of mutations in exons across different tumor types. The plots show that for the tumor types CRC, UCEC and STAD there is a bimodal distribution. The subset of tumor samples with higher number (N) of mutations is considered hypermutated, as indicated (see also Methods and Table S1a).

(B) Relationship between the SCNA level and driver mutations in the DNA damage pathway across tumor types. The relationship between the SCNA level and the presence of at least one functionally relevant mutation in TSGs or OGs

involved in the DNA damage pathway is shown as a boxplot. The p-value (Wilcoxon test) is shown. For each tumor type, the hypermutated samples were excluded (see Methods).

Fig. S2

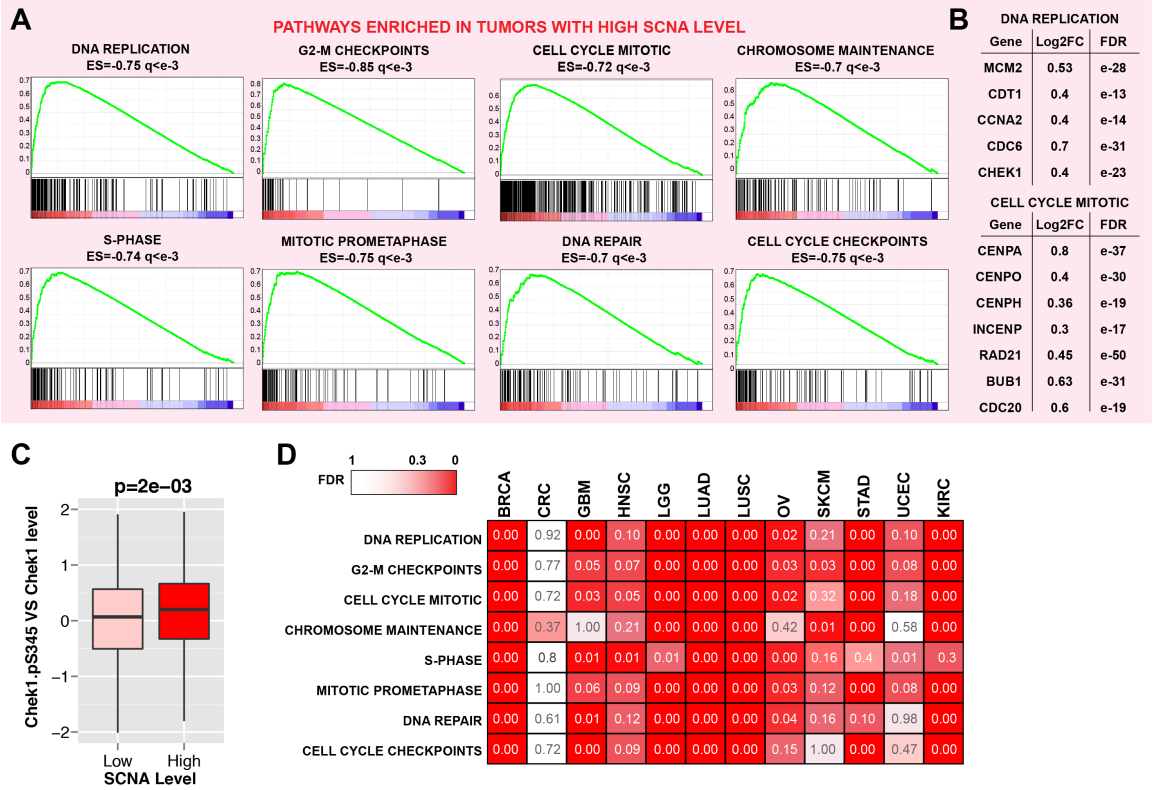

Figure S2

Enrichment in DNA replication, cell cycle pathways and chromosome maintenance in high versus low aneuploidy tumors

(A, B) GSEA analysis on the pan-cancer dataset. RNAseq analysis was performed as a pan-cancer analysis by comparing tumors with high versus low SCNA level and considering tumor type as a covariate (EdgeR package). GSEA plots, ES (enrichment score) and FDRs are shown for representative pathways enriched in high versus low aneuploidy tumors (A). In (B) the log2 fold change (log2FC) between high versus low aneuploidy tumors and corresponding FDR (EdgeR analysis) are shown for representative genes. See also Table S3a-b.

(C) Difference in the ratio between P-Chk1 (S345) and total Chk1 levels in high and low aneuploidy tumors (pan-cancer analysis, normalized per tumor type). The ratio between P-Chk1 and total Chk1 was determined for each tumor sample utilizing the TCGA RPPA dataset (*74*). The p-value for the Wilcoxon test is shown.

(D) GSEA analysis on the tumor type-specific datasets. For each tumor type, RNAseq analysis was performed comparing tumors with high versus low SCNA levels as in (A). GSEA analysis was performed as in (A) and the FDR values for the indicated tumor type and pathway are shown. 0.00 indicates a FDR <e-2. See also Table S4a.

Fig. S3

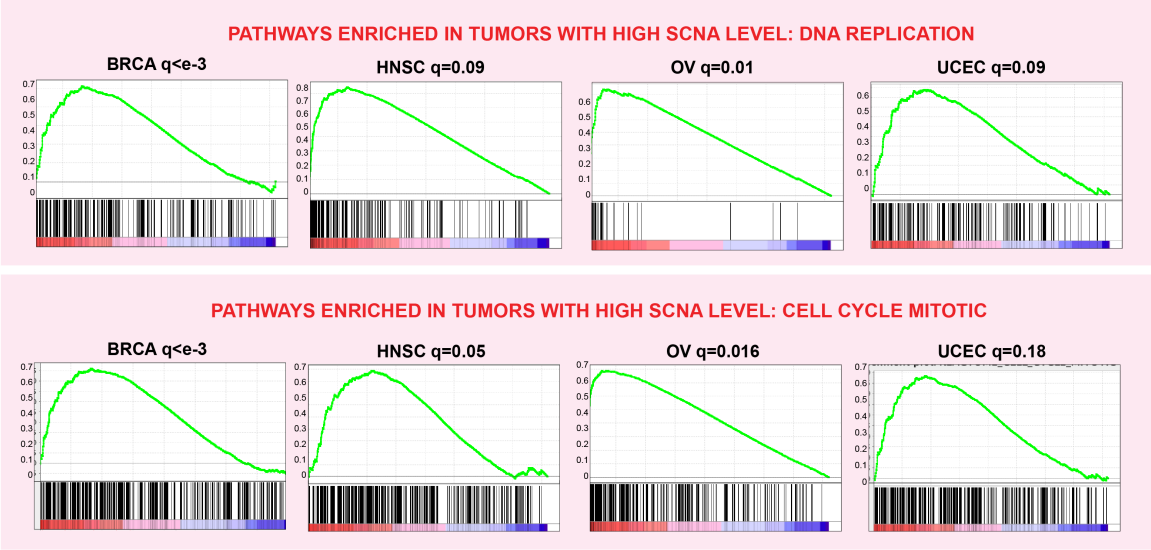

Figure S3

Enrichment in DNA replication and mitotic pathways in high versus low aneuploidy tumors within individual tumor types.

RNAseq analysis was performed comparing high versus low aneuploidy tumors from each indicated tumor type and GSEA was performed as in Fig. S2D. GSEA plot and FDR are shown for representative pathways enriched in high versus low aneuploidy tumors (see also Table 4a).

Fig. S4

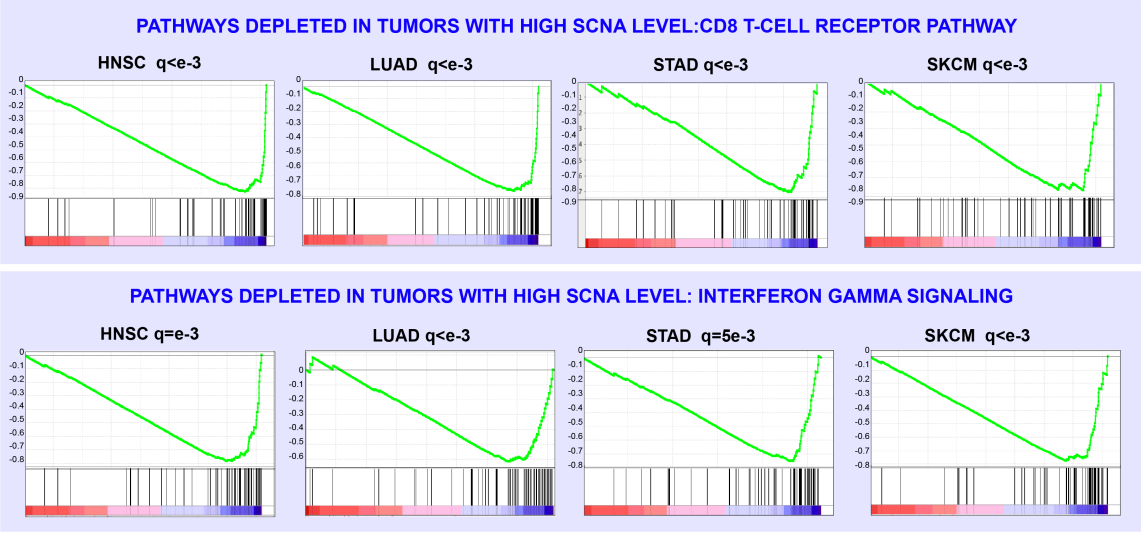

Figure S4

Depletion in the CD8 TCR pathway and the Interferon gamma signaling pathway in high versus low aneuploidy tumors within individual tumor types.

RNAseq analysis was performed comparing high versus low aneuploidy tumors from each indicated tumor type and GSEA was performed as in Fig. 2C. GSEA plots and FDRs for representative pathways depleted in high versus low aneuploidy tumors are shown (see also Table 4b).

Fig. S5

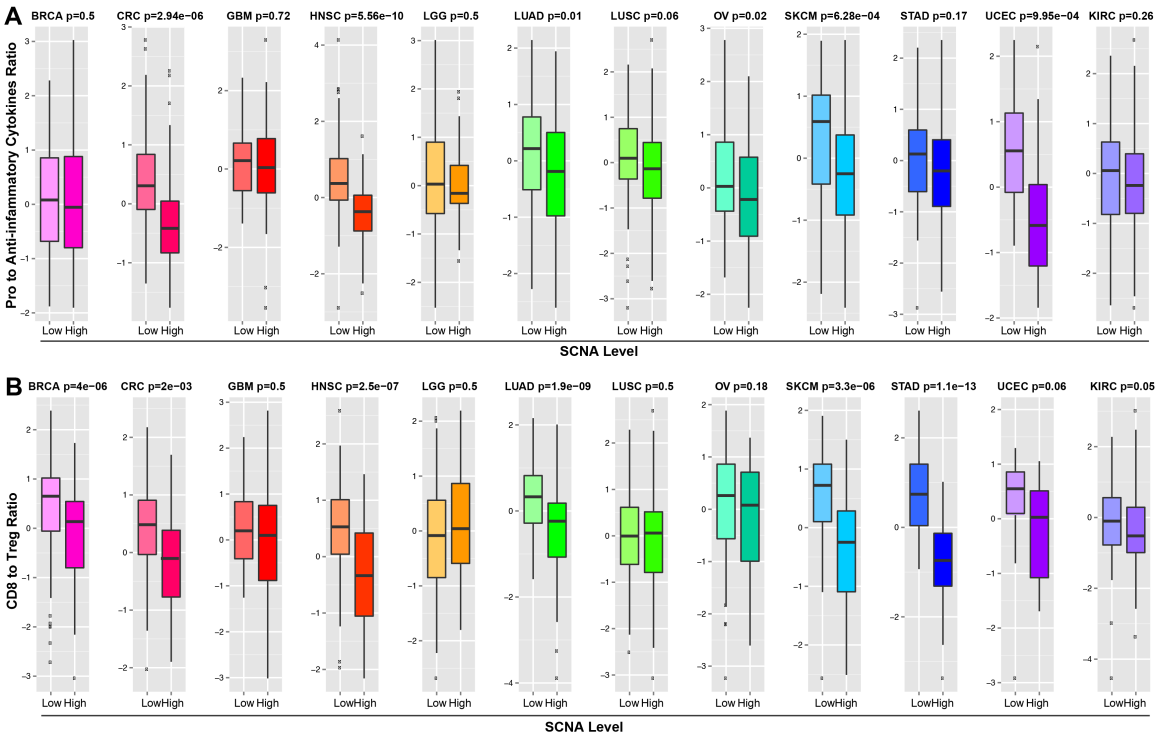

Figure S5

Analysis of specific immune molecules in tumors with high versus low aneuploidy within individual tumor types.

(A) Specific changes of pro-inflammatory and anti-inflammatory gene expression in the pan-cancer analysis. The ratio between the average expression level (log2 transformed RSEM value) of pro-inflammatory (IFNG, IL-1, IL-2) versus anti-inflammatory genes (TGFB1, IL-10, IL-4, IL-11) was calculated in each tumor sample and the change in the distribution of this parameter between tumors with low and high aneuploidy is shown for individual tumor types as boxplots.

(B) The ratio between the average expression level (log2 transformed RSEM value) of the markers specific for CD8 effector T cells versus Treg cells was calculated for each tumor, based on the gene sets used for Fig. 3C (Table S4d). The distribution of this ratio between low and high aneuploidy tumors is shown for individual tumor types as boxplots.

Fig. S6

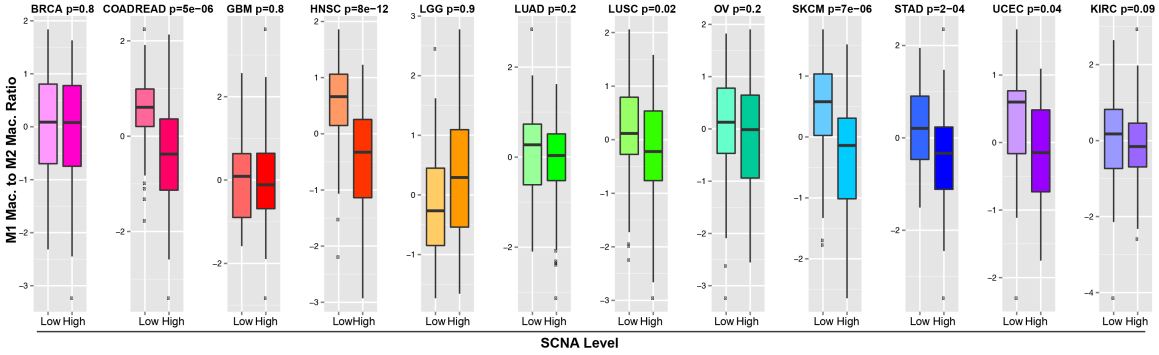

Figure S6

Analysis of the ratio between M1 and M2 macrophages within individual tumor types.

The ratio between the average expression level (log2 transformed RSEM value) of the markers specific for M1 and M2 macrophages was calculated for each tumor, based on the gene sets used for Fig. 3D (Table S4d). The distribution of this ratio between low and high aneuploidy tumors is shown for individual tumor types as boxplots.

Fig. S7

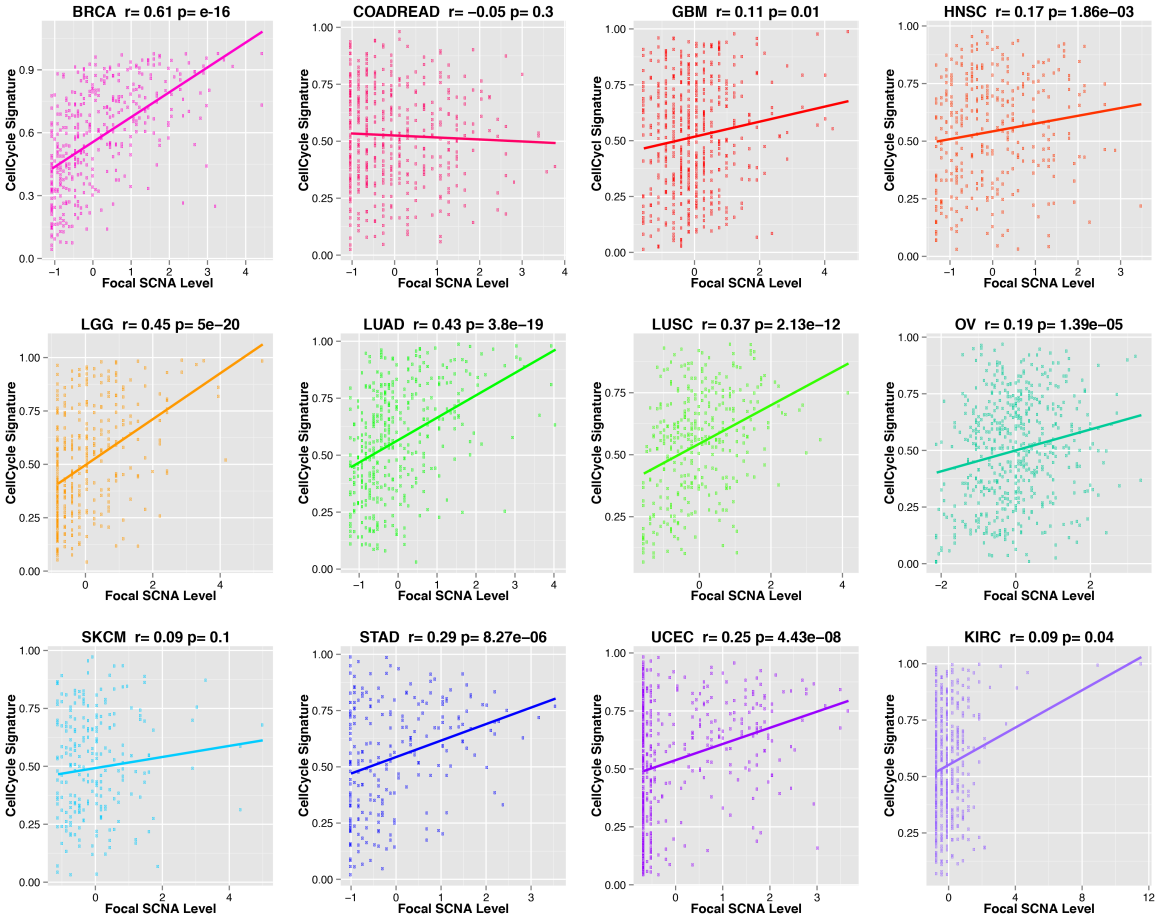

Figure S7

The relationship between the focal SCNA level and the cell cycle signature score in individual tumor types.

The relationship between cell cycle signature score and the focal SCNA score in individual tumor types. For each tumor type a plot is shown, containing the cell cycle signature (y-axis) versus the focal SCNA level (x-axis) in each sample. The Spearman correlation coefficient and p-value are shown.

Fig. S8

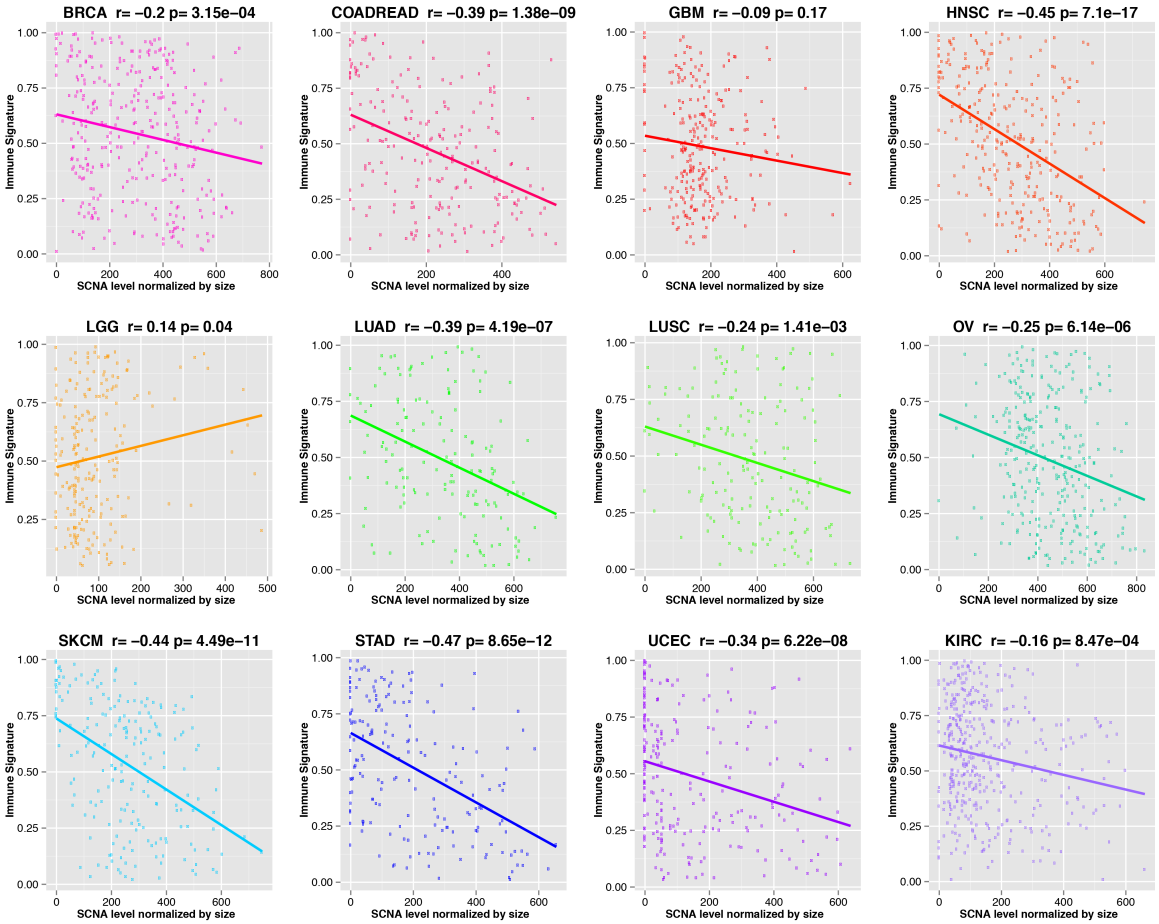

Figure S8

The relationship between the SCNA level normalized by event size and the immune signature score.

The ‘SCNA level normalized by size’ represents the integrated level of SCNAs in each tumor sample. To determine this SCNA level, we considered 800 genomic regions corresponding to cytogenetic bands and for each region we determined its copy number level (amplification/deletion). The ‘SCNA level normalized by size’ represents the sum of these genomic regions deleted or amplified (see Methods). For each tumor type a plot is shown, containing the immune signature score (y-axis) versus the SCNA level normalized by size (x-axis) in each tumor sample. The Spearman correlation coefficient and p-value are shown.

Fig. S9

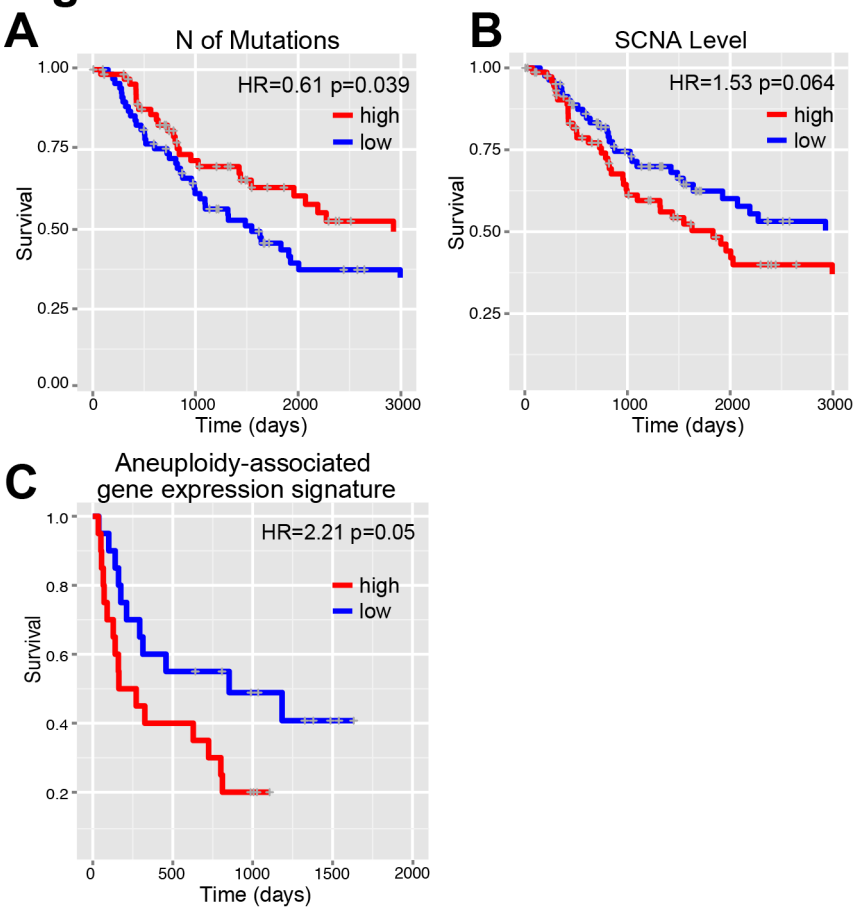

Figure S9

Role of SCNA level and N of mutations in predicting survival in melanoma patients not treated with immunotherapy.

(A, B) Survival analysis for the number of mutations (A) and the SCNA level (B) in melanoma patients from the TCGA dataset not treated with immunotherapy. The number of mutations and the SCNA level were utilized as individual predictors of survival in a univariate Cox proportional hazards models. In all cases, patients were stratified in two groups, utilizing the median of the parameter as a cutoff (upper or lower 50%). HR and Wald test p-values from the Cox proportional hazards model comparing the two groups of patients are shown. Kaplan-Meyer survival curves for patients stratified in the two groups are shown (Table S6c).

(C) The aneuploidy-associated gene expression signature was derived from genes showing a positive correlation with the SCNA level and a negative correlation with the immune infiltrate signature was derived based on the TCGA dataset of melanoma samples (Table S6e). This gene expression signature was utilized to rank the tumor samples from the dataset of melanoma patients treated with immunotherapy (*26*) (based on the average expression level). Survival analysis was then performed by comparing the tumors with a gene expression signature higher or lower than the median level. Kaplan-Meyer survival curves, HR and Wald test p- are shown.

Legends to Supplementary Tables

Table S1: Information on the tumor dataset and SCNA events

Table S1a: Information on the tumor dataset including the abbreviation and description for each tumor type and the total number of samples for each tumor type. This table also contains the median of the estimated purity across samples (median purity estimate) and the noise threshold utilized for SCNA calls (threshold used for SCNA calls) in each tumor type. The median purity estimate was derived from ABSOLUTE calls (*3*, *59*) when available or, when not available, from the pathology report (see Methods). Finally, this table also contains the threshold in the number of mutations in exons to define hypermutated tumors for each tumor type. Samples with a number of mutations in exons higher than this threshold were considered hypermutated samples.

Table S1b: List of focal amplification events derived from GISTIC2 analysis performed on all tumor samples.

Table S1c: List of focal deletion events derived from GISTIC2 analysis performed on all tumor samples.

Table S1d: List of chromosome, arm and focal SCNA events considered.

Table S2: Analysis of mutations in specific pathways

Table S2a: List of TSGs and OGs predicted by TUSON Explorer (*11*) and utilized for different analyses in this paper.

Table S2b: List of TSGs and OGs (from TUSON Explorer) involved in specific cellular pathways utilized for the analyses in Fig. 1C-D, Fig. S1B and Table S2d. For each cancer-related pathway, the list of TSGs and OGs involved in it that pathway are shown.

Table S2c: Tumor type-specific analysis showing the relationship between the number of SCNAs and the mutations in passenger genes, driver genes, and the ratio between number of mutations in drivers over the number of mutations in passengers. The hypermutated samples were excluded (see Methods). The correlation coefficient and p-value between the SCNA level and the number of mutations in the indicated classes of genes are shown. See also Fig. 1B.

Table S2d: For each tumor type, the correlation between the SCNA level and the number of mutations in driver genes (TSGs and OGs) involved in the indicated pathways was derived. P-values and correlation coefficients are shown for each tumor type.

Table S2e: Analysis of the correlation between the SCNA level and the number of mutations in passengers and drivers. This analysis is similar to the one described in Fig. 1B, except the fact that all samples (including hypermutated samples) were included.

Table S3: GSEA analysis of pathways depleted and enriched in tumors with high versus low aneuploidy tumors

Table S3a: The SCNA level was first calculated for all the tumor samples. EdgeR was utilized to compare the tumors with high versus low SCNA level (tumors with SCNA level higher than 70^{th} percentile versus tumors with a SCNA level lower than 30^{th} percentile), considering the tumor type as a covariate. Table S3a contains the results of the EdgeR analysis for each gene. The final score represents the negative log10 of the FDR multiplied by the sign of the log2 fold change (log FC), which was then utilized as the 'weight' to run the GSEA 'weighted' enrichment analysis. A positive Final Score corresponds to genes enriched in high versus low aneuploidy tumors and vice-versa.

Table S3b: Result of the GSEA analysis for the pathways enriched in tumors with high versus low aneuploidy, in a pan-cancer analysis. RNA seq analysis was

performed using EdgeR (Table S3a) and GSEA 'weighted' enrichment analysis was performed.

Table S3c: Result of the GSEA analysis for the pathways depleted in tumors with high versus low aneuploidy, in a pan-cancer analysis. RNA seq analysis was performed using EdgeR (Table S3a) and GSEA 'weighted' enrichment analysis was performed.

Table S4: GSEA analysis of pathways depleted and enriched in single tumor types comparing high versus low aneuploidy tumors

Table S4a: RNAseq analysis was performed with EdgeR for each individual tumor type as for Table S3a, followed by GSEA analysis. The result of GSEA analysis for pathways enriched in tumors with high versus low aneuploidy is shown for the indicated tumor types.

Table S4b: RNAseq analysis was performed with EdgeR for each individual tumor type as for Table S3a, followed by GSEA analysis. The result of GSEA analysis for pathways depleted in tumors with high versus low aneuploidy is shown for the indicated tumor types.

Table S4c: Details on the immune cell types utilized for the analysis of gene expression within the Immgen database (https://www.immgen.org).

Table S4d: List of genes utilized as specific markers of the indicated immune cell types and derived from the analysis based on the Immgen database.

Table S5: Relationship between arm-chromosome SCNAs and focal SCNAs with the cell cycle and the immune signature scores.

Table S5a: List of genes utilized for the calculation of the cell cycle signature score based on gene expression profile.

Table S5b: List of genes utilized for the calculation of the immune signature score based on gene expression profile. Note that this signature mainly represents CD8 T cells and NK cells-mediated cytolytic activities.

Table S5c: Logistic regression for the prediction of the cell cycle signature score and the immune infiltrate signature score was performed utilizing the arm-chrom SCNA score and the focal SCNA score as parameters. The β-coefficients and p-values are reported in this table.

Table S5d: For each genome segment (800 genomic regions corresponding to cytogenetic bands), the frequency of amplification or deletion was determined, both at the focal and arm-chromosome level (see Methods) for each tumor type. The correlation (correlation coefficient and p-value) between the focal and arm-level SCNAs is indicated for each tumor type.

Table S5e, f: *Lasso*-mediated prediction of the immune infiltrate. For each tumor type, *lasso* was utilized to identify the best parameters predicting the cell cycle (Table 5e) or the immune infiltrate signature score (Table 5f) on the training set. The selected parameters were then utilized to refit a logistic regression model on the training set and the corresponding β-coefficients are shown for each indicated parameter and tumor type. A coefficient of 0.00 refers to parameters that were not selected by *lasso*. The resulting model was applied to the test set and area under the curve of the ROC (ROC-AUC) is shown for each tumor type. The number of mutations was considered as log-transformed and standardized. TP53 and age were considered as binary parameters, and all the other parameters were standardized. NAs indicate that the corresponding parameters were not applicable. The SCNA level was normalized within histological subtypes.

Table S5g: Correlation between the SCNA level and the immune infiltrate signature score after normalization for the purity level for each sample. A threshold for the SCNA calls was determined for each patient based on its estimated purity level (from the pathology report) (Table 1). Arm and Chrom

SCNA level was determined and its correlation (Spearman) with the immune signature score was determined (Table 2).

Table S6: Survival analysis in datasets of immunotherapy in melanoma patients.

Table S6a: Survival Analysis in melanoma patients after anti-CTLA-4 treatment using the indicated parameters to predict survival. The data were derived from the following study: Van Allen et al., Science, 2015 (*26*). In all cases (except the one called 'Survival analysis: N mutations, threshold 100'), the patients were divided into two groups based on the median of the parameter or risk score and the Cox proportional hazards model was applied. In the case called 'Survival analysis: N mutations, threshold 100', a threshold of 100 mutations was utilized to group the patients. The hazard ratio (HR) and the Wald test p-value were determined. The proportional hazard assumption was also tested and the corresponding p-value is shown.

Table S6b: Survival Analysis in melanoma patients after anti-CTLA-4 treatment using the indicated parameters to predict survival. The data were derived from the following study: Snyder et al., NEJM, 2014 (*25*). A similar analysis to the one described in Table S6a was performed.

Table S6c: Survival Analysis in melanoma patients from TCGA using the total number of mutations, SCNA level or immune signature score as predictors. In all cases, the patients were divided into two groups based on the median of the parameter or risk score and the Cox proportional hazards model was applied. The hazard ratio (HR), corresponding Wald test p-value and C-Statistics were determined. When indicated, multiple parameters were included in the same model.

Table S6d: Interaction analysis between SCNA score and immunotherapy treatment. The TCGA dataset of melanoma patients not treated with immunotherapy and the dataset of patients treated with immunotherapy (*25*, *26*) were combined together. Multi-variable Cox proportional hazard model was

applied considering the combination of low SCNA level (bottom 50%) and immunotherapy treatment and combination of high N of mutations and immunotherapy as predictors (survival analysis 1). In addition multi-variable Cox proportional hazard model was applied also considering the same predictors in analysis 1 excluding the combination of SCNA level and immunotherapy and combination of N of mutations and immunotherapy (survival analysis 2).

Table S6e: Gene set showing a positive correlation with the SCNA level and a negative correlation with the immune signature score was derived based on the TCGA dataset of melanoma samples (Table S6e). This score was used for the survival analysis shown in Fig. S9C.

Table S7: TCGA dataset with clinical and molecular parameters.

TCGA dataset with clinical and molecular parameters, including SCNA level, mutation numbers, cell cycle and immune signature expression scores.

Table S8: Dataset with clinical and genomic parameters for the immunotherapy datasets.

Table S8a: Dataset of genomic and clinical parameters from the study of Van Allen et al., 2015 (*26*), including SCNA level.

Table S8b: Dataset of genomic and clinical parameters from the study of Snyder et al., 2014 (*25*),including SCNA level.

Additional issues regarding the mechanism of immune evasion addressed by the supplemental figures.

One issue is whether dysregulation in proteasomal turnover could impact the immune infiltrate. We reasoned that an increase in the flux of unstable proteins through the proteosome might impact the presentation of neoantigens on MHC Class I in tumor cells with high levels of aneuploidy. Since the number of normal proteins vastly exceed the number of mutated proteins, we hypothesize that, in high aneuploidy tumor cells, the majority of unstable proteins funneled through the proteasome are made up of normal (*e.g.* not mutated) peptides. The resulting increase in self-antigens may compete with tumor neoantigens to reduce their presentation on MHC. The balance of this competition has the potential to impact CD8+ T cell mediated killing and immune infiltration if MHC I levels become limiting in the same way that reduced MHC I function might. We refer to this as the 'flooding" hypothesis. If aneuploidy occurs early in tumors, which has been argued based recent analyses of clonal evolution in cancer (*3*, *71*, *72*), then the neoantigens that accumulate later in evolution will be at an even greater disadvantage, being produced in an environment already 'flooded' by aneuploidy-derived non-antigenic self-peptides. The flooding hypothesis does not exclude the possibility that specific arm SCNAs (and/or focal SCNAs, such as PD-L1 and PD-L2, in some cases) can also contribute to immune evasion by the tumor. In fact, in HNSC and STAD focal SCNAs seem to play a role together with the arm/chromosome SCNAs in predicting the immune infiltrate.

It is also possible that proteotoxic stress generated by aneuploidy could affect ubiquitin pools or impair the ER compartment to affect dynamics of MHC function or antigen loading in general to alter the immune infiltrate. Taken together, we propose a hypothetical and speculative explanation where it is not only the number of neoantigenic mutations *per se* that control the immune infiltrate but possibly the amount of neoantigenic peptides that can be presented on the surface and that this level may be controlled in part by the state of aneuploidy in the tumor.